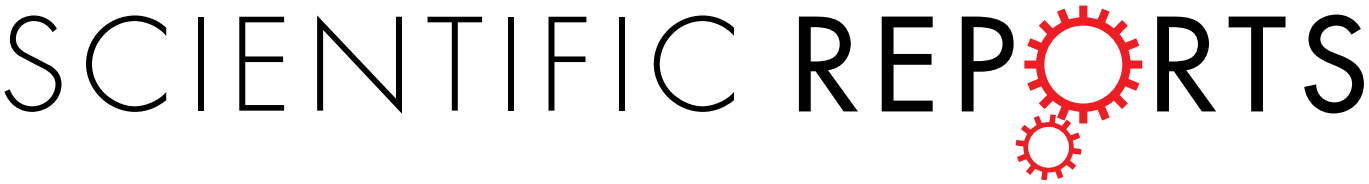

OPEN

Received: 4 November 2016
Accepted: 5 April 2017
Published online: 12 May 2017

Preparation of Nanowire like WSe_2-Graphene Nanocomposite for Photocatalytic Reduction of CO_2 into CH_3OH with the Presence of Sacrificial Agents

Asghar Ali & Won-Chun Oh

A nanowire-like WSe_2-graphene catalyst was prepared via ultra-sonication and was tested in terms of the photocatalytic reduction of CO_2 into CH_3OH under irradiation with UV/visible light. The prepared nano-composite was further characterized via XRD, SEM, TEM, Raman and XPS. The photocurrent analysis was further tested for its photocatalytic reduction of CO_2 using gas chromatography (GCMS-QP2010 SE). To further improve the the photo-catalytic efficiency, a sacrificial agent (Na_2S/Na_2SO_3) was added to the WSe_2-graphene nanocomposite and was found to improve the photo-catalytic efficiency, with the methanol yield reaching 5.0278 μmol $g^{-1}h^{-1}$. Our present work provides a convenient way to prepare nanomaterials various morphologies that have future applications for environmental remediation.

The increase in the amount of the CO_2 emissions in the environment has reached an alarming level, greatly contributing to global warming[1], and in the last few decades, the shortage of fossil fuel resources has resulted in an increased demand for energy production from different sources, including photovoltaic and photocatalytic H_2 production. One such technology is photocatalytic CO_2 reduction, which is a most valuable approach to overcome both global environmental and energy problems due its low cost, clean energy production, and environmental friendliness[2,3]. In particular, the photocatalytic reduction of CO_2 can convert noxious gasses (carbon dioxide) into profitable solar fuels, i.e., CO, HCHO, CH_3OH, and CH_4 by using solar energy[4,5]. To date, many photocatalysts such as TiO_2, CdS, g-C_3N_4, ZnO and Bi_2WO_6 have been shown to achieve the photo reduction of CO_2[6–10]. Unfortunately, there are limits to the practical applicability of these semiconductors because the efficiency of the CO_2 conversion into useful products is very low due to many factors of the CO_2 reduction process, e.g., band gap tuning, charge carrier recombination, and light utilization[11]. Due to the wide band gap energy, most materials are unable to absorb visible light, and on the other hand, small band gap semiconductors exhibit a fast recombination phenomenon. To overcome this and to find an achievable process, highly efficient, low cost transition metal dichalcogenides (TMDC) have been investigated[12–15]. The generalized formula for TMDs is MX_2, where M = transition metal element of group 4, 5 or 6 and X represents a chalcogen. Tungsten diselenide (WSe_2) is a semiconductor that belongs to the TMDC family. Its structure consists of Selenium and tungsten held together by a weak van der Waals force that allow the material to be exfoliated into monolayers[16,17]. Moreover WSe_2 is a layered semiconductor with a small band gap of approximately 1.6 eV[18]. It has unique electrical transport performance, and its use was recently reported in many advanced energy storage applications, such as in superconductors[19], lithium ion batteries[20], photodetectors[21], and photocatalytic hydrogen production[22] in solar cells. Furthermore, Li, Yanguang *et al.* and Merki, Daniel *et al.* indicated that both the theoretical calculation and experimental results for the hydrogen evolution reaction of transition metal dichalcogenide (WSe_2) materials appears to be from active edge sites that play an important role in hydrogen evolution reaction catalysis[23,24]. However, due to the intrinsic interlayer *Van der Waals* attraction, the layered TMDC materials can be easily re-stacked as a result of reducing the active edge sites. Therefore, to improve photocatalyitc activity, the TMDC (WSe_2) materials are combined with 2D carbon material such as graphene.

Department of Advanced Materials Science & Engineering, Hanseo University, Seosan, 31962, Korea. Correspondence and requests for materials should be addressed to W.-C.O. (email: wc_oh@hanseo.ac.kr)

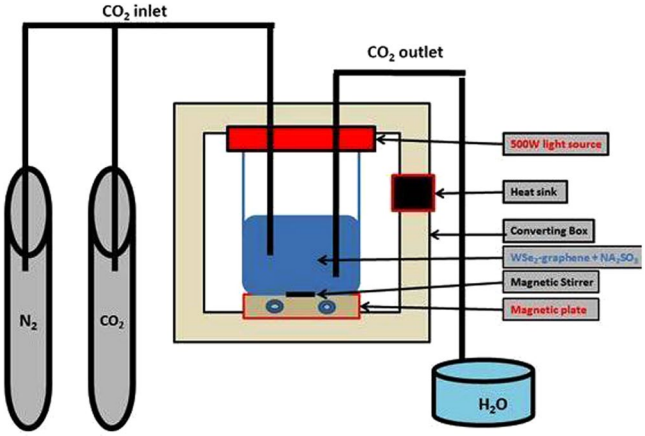

Figure 1. The schematic diagram of CO_2 reduction device.

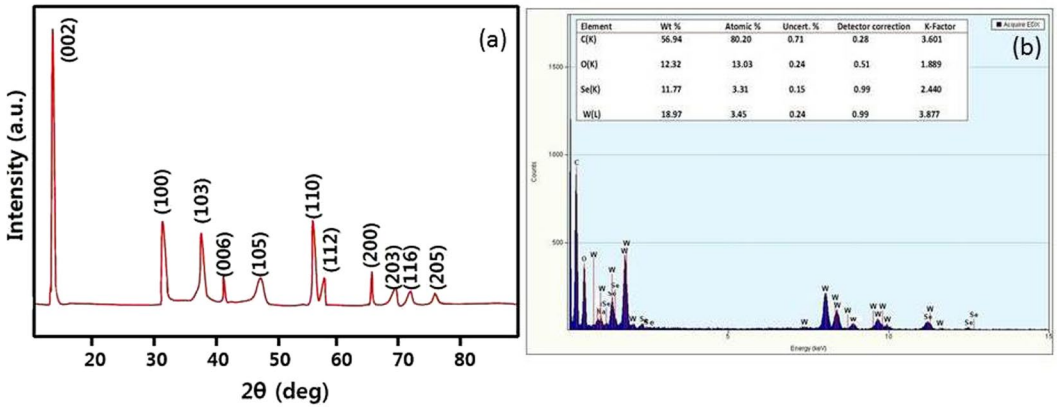

Figure 2. (**a**) XRD pattern and (**b**) EDX of WSe_2-graphene composite.

Graphene has unique properties, including a large surface area, good conductivity, and high flexibility, and it is used in high-performance energy storage devices[25,26]. Therefore, coupling with a photocatalyst may improve the photocatalytic reduction efficiency of CO_2 to fulfill the practical requirements. Liange *et al*. first described that coupling with a semiconductor is one of the best ways to boost the photocatalytic reduction efficiency of CO_2[27]. Recently, graphene coupled with TMDCs (WSe_2) was reported for the hydrogen evolution reaction (HER)[28], high-performance oxygen reduction reaction (ORR)[29] and in a superconductor[30]. However, the WSe_2 chalcogenide family has not yet been analyzed for the photocatalytic reduction activity of CO_2. In the present study, we report on WSe_2-graphene nano composites prepared via ultra-sonication. The prepared samples (WSe_2-graphene) were used for CO_2 reduction, and the results exhibit a high efficiency for photo catalytic CO_2 conversion under UV and visible light irradiation.

Results and Discussion

Characterization of catalytic materials. The XRD patterns of the WSe_2-graphene nanocomposites is shown in Fig. 2(a), the diffraction peaks at 13.54, 32.50, 38.45, 41.86, 47.75, 56.25, 58.10, 66.77, 69.45, 72.55 and 76.78° correspond to (002), (100), (103), (006), (105), (112), (200), (203), (116) and (205) directions, respectively ($a = b = 0.329$ nm, $c = 1.298$ nm, JCPDS PDF# 00-38-1388)[28,29]. However, no other diffraction peaks form any other chemical species were observed in the prepared sample. For the GO analysis, a sharp peak (002) occurs at 13.44°, revealing that the graphite power was converted into graphene oxide by expanding the d-spacing from 3.5 to 6.78 Å[31,32]. Moreover, the results indicate that the XRD signals of GO are very weak and are overlapped with those of WSe_2-graphene at 13.54°. Therefore, the measurements were unable to detect the weaker diffraction peaks of GO[33]. Further EDX spectra confirm the presence of the main elements in the catalyst composites. The Fig. 2(b) shows the presence of the prime elements C, O, W, and Se, The C elemental peak is derived from graphene sheet, and W, Se and O are the precursor material.

SEM observations were carried out to investigate the surface and structural morphology. Figure 3 shows the SEM images of WSe_2-graphene at different magnifications. Figure 3(a) shows the wire-like and nanoscale WSe_2 morphology composed of interlaced and ultrathin nanosheets uniformly dispersed on the graphene nanosheet. Figure 3(b) and (c) show that graphene has an irregular structure that is broken off in different directions. Figure 3 also indicates that the WSe_2 nanowires extensively grow on the surface of the graphene nanosheet. Figure 3(c)

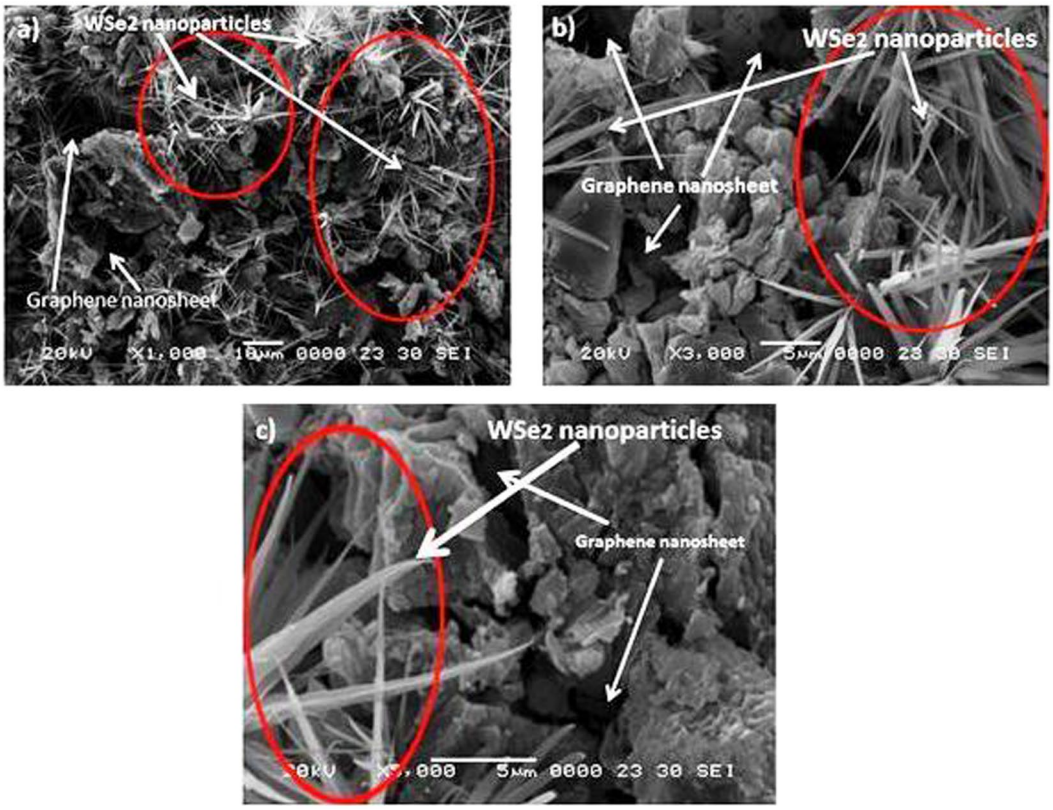

Figure 3. SEM imges of WSe_2-graphene composite with different mignification.

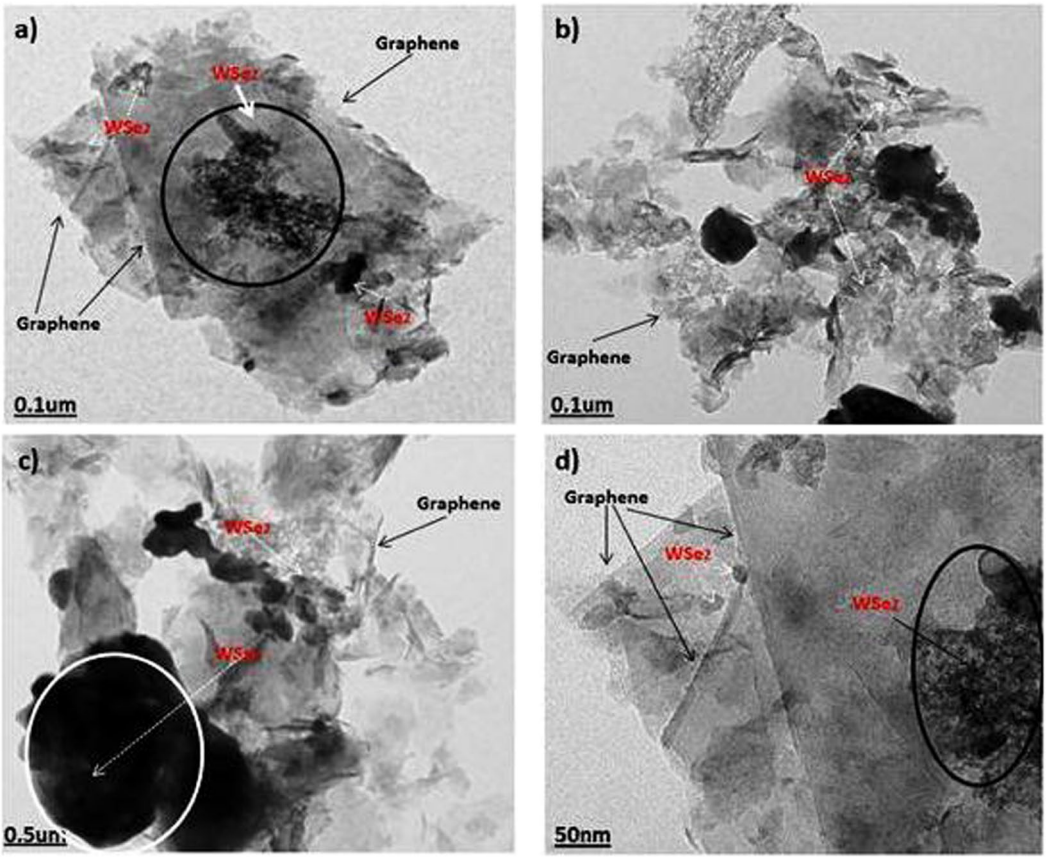

Figure 4. TEM image of WSe_2-graphene.

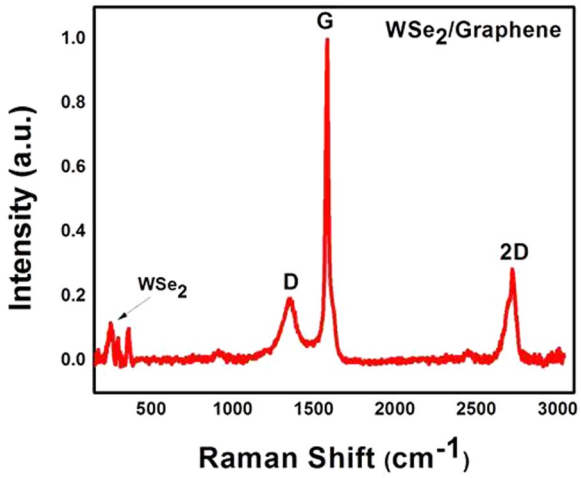

Figure 5. Raman spectra of the WSe_2-graphene nanocomposite.

depicts bright nanowire WSe_2 shapes that are properly coated on the graphene surface, indicating that graphene nanosheets provide a good platform for the nucleation and successive growth of WSe_2 layers, and growth on WSe_2 in graphene is possible due to the precursors that are attached to the graphene oxide through functional groups [23,34–36]. Figure 4(a–d) shows transmission electron microscopy (TEM) that further confirms the morphology and shape of the WSe_2-graphene nanocomposites. Figure 4(a–c) shows the WSe_2-graphene nanocomposites at different magnifications. The WSe_2 is clearly seen to have dark imaged compounds that are almost very small in a spherical form, layer form, and a highly agglomerated structure attached to the surface of the graphene sheets. Moreover, several layers of the WSe_2 are covered with the graphene nano sheets, and the average size of the WSe_2 is measured to be approximately 6 to 10 um using the ImageJ software.

Figure 4(d) shows the formation of single-crystalline and few-layered WSe_2 nanosheets. Different WSe_2 flakes indicating that the particles sizes fluctuate between 30 nm to 190 nm. When compared to the bulk material, the size of the WSe_2 layers decreases, which is may be due to the discontinuity of the particles induced by sonication and particle selection by centrifugation[37]. The precise structural properties of the WSe_2-graphene were analyzed via Raman spectroscopy. Figure 5 provides comprehensive detail of the GO and WSe_2 nannocomposites (e.g., crystal structure and no. of layers), Fig. 5 shows the Raman signature energy band of the WSe_2 located at 200 to 400 cm^{-1}. The typical Raman spectra for WSe_2 shows a band at the A_1g (out-of-plane) (255 cm^{-1}) and E_12g (inplane) mode (250 cm^{-1})[38].

Figure 5 also shows that the characteristics of the graphene Raman shifts for the D, G, and 2D bands. The D band is located at 1360 cm^{-1}, which shows the presence of disorder in the atomic arrangements or edge effect of graphene, while the G band appears at 1590 cm^{-1}. Both the G and D band show the vibration of the carbon atoms in disorder or defect sites and the in-plane vibration of sp^2 and sp^3 bonded carbon atoms[39]. These two bands (D 1360 cm^{-1}, G 1590 cm^{-1}) indicate an interaction between rGO and selenide nanosheets, which improves the stability of the catalyst interface and provides a high stability for the nanocomposites. A 2D band appears at 2690 cm^{-1} to express the degree of graphitization. Moreover, the 2D band is smaller than the G band in our spectrum, which indicates the presence of a few layers of graphene sheets[40–43].

XPS measurements were carried out to assess the elemental composition of the WSe_2-graphene nanocomposite. Figure 6(a) shows the XPS spectrum, which indicates the presence of W, Se, C and O and shows the formation WSe_2-graphene nanocomposite. Figure 6(b) shows the XPS spectrum of W and the binding energies of $W4f_{7/2}$, $Wf_{5/2}$ and $W5p_{3/2}$ at positions of 31.90, 34.80 and 37.90 eV, respectively. The $W4f_{7/2}$ and $Wf_{5/2}$ binding energy peaks express the elemental chemical binding state of W, while the peak positioned at 37.70 eV is attributed to the core level of $W5p_{3/2}$ from WO_3 due to the partial oxidation of the WSe_2 layers[44,45]. The binding energy for the Se $3d_{3/2}$ core level peak of 54.90 eV confirms a lattice Se^{-2} of the WSe_2-graphene hybrid (Fig. 6c). The core peak level of Se3d between 50 to 56 eV shows the absorbance of pure Se in a catalysts, which is conclude that WSe_2-graphene nanocomposite is free from any impurity[46,47]. Figure 6(d) shows the core level XPS spectrum of the O1s, peak located at 532.90 eV, which shows the carbonyl and carboxyl groups, while the C1s (Fig. 6(e)) spectrum is located at 284.5 eV. These results show that the spectra can fit with oxygen containing functional groups (C-C, C-O), which is evident in the reduction of GO to rGO[48–52].

The UV-vis diffuse reflectance spectrum of the WSe_2-graphene nanocomposite was displayed in Fig. 7(a). The band gap energy value was achieved where the straight line approaching the curve intersects the horizontal axis. As the results from Fig. 7(a), the band gap energy values of the WSe_2-graphene nanocomposite was 2.68 eV. The photoelectrochemical current response was investigated by employing different materials to decorate the ITO sheet used as a photoanode. The photocurrent of each prepared sample was calculated in a 0.1 M KCl solution containing 0.1 M TEA under "on-off" light illumination cycles at a bias of 0 V vs. Ag/AgCl, as shown in Fig. 7(b). The photoresponse for graphene was non-existent because graphene could not be excited, as shown in curve a[53] to the nature of graphene, which requires further reduction steps to generate a photocurrent signal[54]. This Fig. 7(b) displays the photocurrent response of the ITO/WSe_2-graphene based on time, which was repeatedly measured

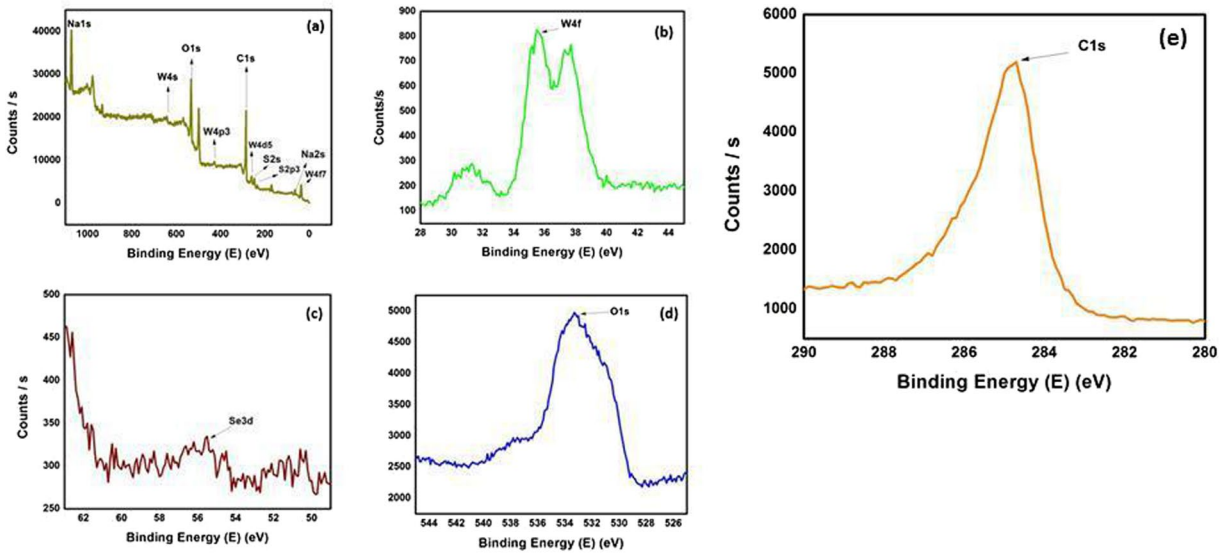

Figure 6. XPS spectra of the WSe_2-graphene nanocomposite: (**a**) survey scan spectra (**b**) W4f (**c**) Se3d (**d**) O1s and (**e**) C1s.

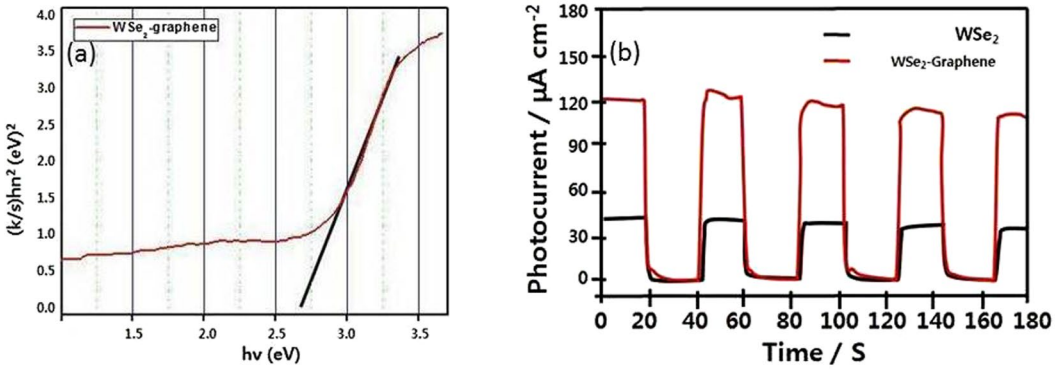

Figure 7. DRS of the WSe_2-graphene composite and photocurrent measurement with pure WSe_2 semiconductor (**a**) and WSe_2-graphene modified photoelectrodes (**b**).

five times at 20-s intervals under visible irradiation. No current was observed in the dark, which clearly suggests that no photoinduced charge separation took place. When the light was turned on, the photocurrent intensity was significantly increased to 121.21 μA. This may have been due to the photoinduced electron–hole separation at the WSe_2, in which the holes were scavenged by the TEA, and graphene acted as an electron transfer medium. Thus, the electrons were transported to the ITO electrode, resulting in photocurrent generation. The electrode showed a pronounced and stable photocurrent response during the light "on-off" condition, which it maintained.

Photocatalytic performance. We assessed the photocatalytic activity of the pure WSe_2 and WSe_2-graphene composites for 48 h during UV ($\lambda > 300$) and visible ($\lambda > 400$) light irradiation, and every 12 h interval sample withdraw manually from the reactor using a gas-tight syringe, then the collected sample was centrifuged and characterized via gas chromatography. Figure 8 displays the CH_3OH yield for the pure WSe_2 and WSe_2-g nanocomposites. The control experiment determined that no methanol yield was produced in the absence of photocatalysts or light irradiations or both. The gas chromatographic study shows that only CH_3OH was successfully achieved as a reduction product. Furthermore, graphene is an electron donor for the reduction of CO_2 as a substitute carbon source to produce CH_3OH, and H_2O was a reactant of the CO_2 reduction. Figure 8(a) shows that the effect of the photocatalytic reduction of CO_2 with pure WSe_2 and WSe_2-graphene under UV light was higher than that for the same composite under visible light.

The methanol yields and quantum yields for the WSe_2-graphene nanocomposite with different time intervals and different conditions under UV/Visible light irradiation are shown in Tables 1 and 2. The methanol yield and quantum yield with WSe_2-graphene (12 h), WSe_2-graphene (24 h), WSe_2-graphene (36 h) and WSe_2-graphene (28 h) under visible light were 2.2434 (0.3285), 2.7021 (0.4435), 3.3243 (0.5346) and 3.5509 (0.5779) μmol $g^{-1}h^{-1}$, and under UV light were 2.8854 (0.4596), 3.1835 (0.3165), 3.7778 (0.6040) and 4.3257 (0.7053) μmol

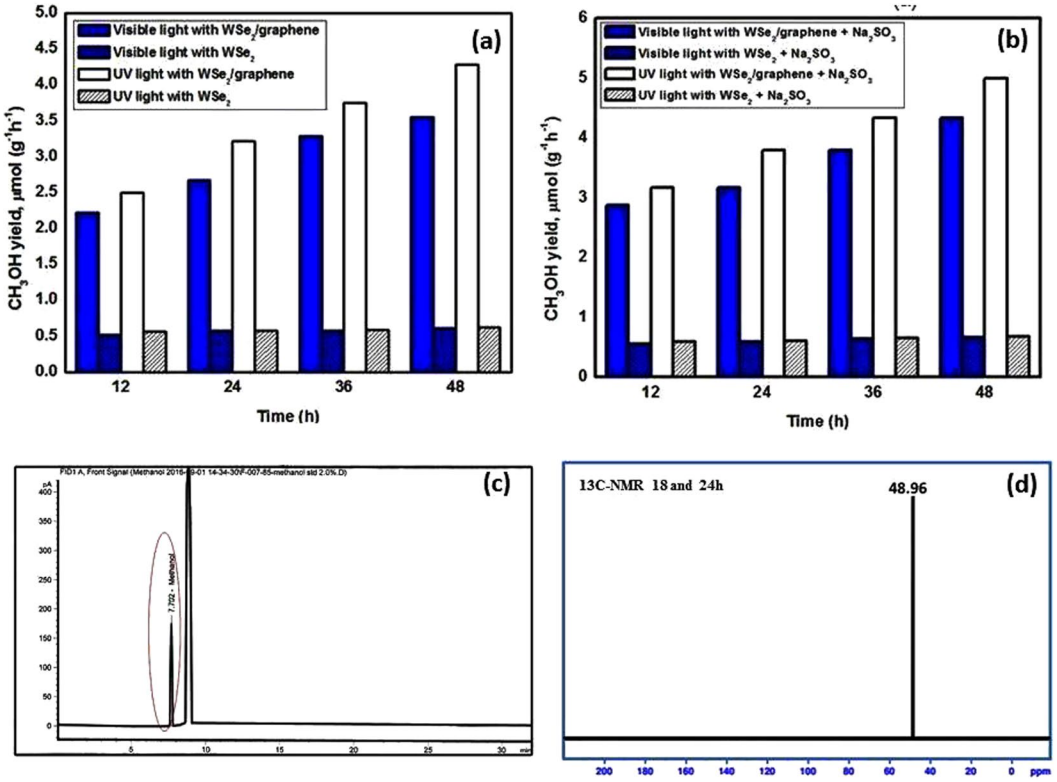

Figure 8. The methanol yields in the photocatalytic reduction of CO_2 under UV/visible light irradiation by using pure WSe_2 and WSe_2-graphene nanocomposits as phtocatalyst (**a**) without Na_2SO_3, (**b**) with Na_2SO_3 (**c**) GC chromatogram of photoreaction using WSe_2-graphene, after 48 h and (d) 13 C NMR (Proton decoupled).

WSe_2-graphene (visible light)	CH_3OH yields ($\mu mol\ g^{-1}\ h^{-1}$)	Quantum yields (QE)
WSe_2- graphene (12 h)	2.2434	0.3285
WSe_2- graphene (24 h)	2.7021	0.4435
WSe_2- graphene (36 h)	3.3243	0.5346
WSe_2- graphene (48 h)	3.5509	0.5779
WSe_2- graphene + Na_2SO_3 (visible light)	**CH_3OH yields ($\mu mol\ g^{-1}\ h^{-1}$)**	**Quantum yields (QE)**
WSe_2- graphene (12 h)	2.8854	0.4596
WSe_2- graphene (24 h)	3.1835	0.3165
WSe_2- graphene (36 h)	3.7778	0.6040
WSe_2- graphene (48 h)	4.3257	0.7053

Table 1. Methanol Production condition with methanol yields and quantum yields under visible light.

WSe_2- graphene (UV light)	CH_3OH yields ($\mu mol\ g^{-1}\ h^{-1}$)	Quantum yields (QE)
WSe_2- graphene (12 h)	2.5134	0.3776
WSe_2- graphene (24 h)	3.2686	0.4294
WSe_2- graphene (36 h)	3.7746	0.5672
WSe_2- graphene (48 h)	2.3523	0.3535
WSe_2- graphene + Na_2SO_3 (UV light)	**CH_3OH yields ($\mu mol\ g^{-1}\ h^{-1}$)**	**Quantum yields (QE)**
WSe_2- graphene (12 h)	3.1848	0.4115
WSe_2 - graphene (24 h)	3.7765	0.5606
WSe_2- graphene (36 h)	4.3246	0.6530
WSe_2- graphene (48 h)	5.0278	0.8159

Table 2. Effect of preparation method on methanol yields and quantum yields under Uv light.

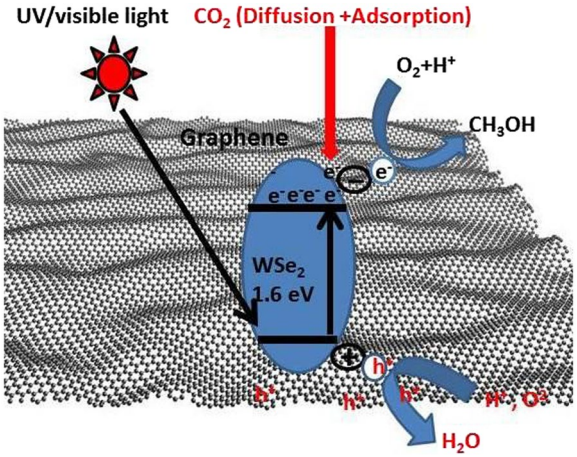

Figure 9. Mechanism study of photocatalytic reduction of CO_2.

$g^{-1}h^{-1}$, respectively. Na_2SO_3 was used as a sacrificial reagent to further enhance the catalytic activity of the binary graphene-based nanocomposites in the photoreduction of CO_2, as shown in Fig. 8. Figure 8(b) shows that the efficiency of the methanol yield of the pure WSe_2 and WSe_2-graphene nanocomposite under UV/visible light is almost two times greater than that of the nanocomposite without using scavenger (Na_2SO_3), and Fig. 8(c) shows a GC calibration curve for the quantification of methanol after 48 hours. The sacrificial reagent plays a crucial role in attaining the stability of the photocatalysts because of the well-known process of photocorrosion of sulfides. For further confirmation of final product CH_3OH, the products were recovered after 18 h and 24 h of irradiation and analyzed by 13 C NMR (Proton decoupled) (Fig. 8d). A single peak was obtained at 48.96 ppm for both, as it is due to methanol, it is verified that photocatalytic conversions of CO_2 yield mainly CH_3OH. It is also substantiated by GC. For stability and recyclability, the WSe_2-graphene nanocomposite was tested for photocatalytic conversion of CO_2 into CH_3OH under UV/Visible light irradiation. The WSe_2-graphene (48 h) was reused for six consecutive runs, and only a minor change in the CH_3OH yield rate was found, indicating that the prepared nanocomposite highly stable and can be used for a continuous photocatalytic reduction system of CO_2.

A further explanation of the proposed photocatalytic mechanism is given in Fig. 9, which shows that the WSe_2 nanomaterial absorbs light of the solar spectrum and creates photo-generated charge carriers (holes and electrons). However, due to the narrow bandgap of the WSe_2 nanocomposite, these electron-holes recombine very quickly, and their photocatalytic efficiency is therefore limited. To improve the photocatalytic efficiency, the WSe_2 nanocomposite was attached to a graphene nanosheet since graphene is an electron accepter/transporter that plays an important role in the separation of the transport electron-hole pairs in the binary system[55]. The excited electron and hole in the conduction band of WSe_2 can be conveniently shifted to the graphene nanosheet, which decelerates the recombination of the electron-hole pairs and thus promotes the electron transport to the catalytic sites for the photo reduction of CO_2. The graphene with a large surface area and many defective sites absorbs the CO_2, and the photo-generated electrons on the WSe_2 are transmitted to the catalytic sites of the graphene and then reduce the absorbed CO_2 into CH_3OH[2,56]. However, the photocatalytic reduction mechanism contains a series of water oxidation and the reduction processes, as shown in Fig. 9. The photo-induced holes on the WSe_2-g VB could absorb water molecules to form hydroxyl radicals ($OH^{\cdot}$), and then the hydroxyl radicals further oxidize the protons (H^+) and oxygen. In the meantime, electrons in the conductor band transfer and absorb CO_2 to form $^{\cdot}CO^{-}_{2}$. The $^{\cdot}CO_{-2}$ reacts with ·H radical, which then leads to the formation of a series of radicals, finally producing CH_3OH.

Reaction Mechanism.

$$WSe_2 + hv \rightarrow WSe_2(e^- + h^+)$$
$$WSe_2(h^+) + H_2O \rightarrow H^+ + O\dot{H}$$
$$\text{Graphene}(e^-) + O_2 \rightarrow O_2^{\cdot}$$
$$\text{Graphene}(2e^-) + 2H^+O_2 \rightarrow H_2O_2$$
$$H_2O_2 + \text{Graphene}(e^-) \rightarrow O\dot{H}$$

CO_2 reaction.

$$2CH_3OH + 3O_2 \rightarrow 2CO_2 + 4H_2O$$
$$2CO_3 + H_2O + 2e^- \rightarrow HCO_2^- + HCO_3^-$$

Methods

Experimental setup and Materials. Tungsten (VI) oxide (WO_3), selenium powder (Se, 99%), ammonium hydroxide (NH_4OH, 25–28%), Sodium sulfite ($Na_2SO_3 \cdot 7H_2O$, 95%), Nitric acid (HNO_3) and ethyl alcohol (94%) were purchased from Duksan Pure Chemical Co. Ltd., Korea. All chemicals were used without further purification, and all dilutions were carried out using distilled water.

Preparation of Graphene. Graphene oxide was prepared in the laboratory following Hummer-Offeman's method, as previously reported in the literature[57, 58]. A typical preparation method for graphene is as follows. First, 20 g of natural graphite and H_2SO_4 (450 ml) are put in de-ionized (DI) water and are stirred continuously for one hour at 0 C. After that, 45 g of $KMnO_4$ are slowly mixed with the solution (graphite + H_2SO_4) and are constantly stirred at a temperature of 35 °C until it becomes a dim brownish color. Then, the container is sealed and kept at 100 °C with vigorous stirring for 30 min. Meanwhile 20% H_2O_2 is added drop wise within 5 min. After that, the solution is washed with acetone and 10% HCl several times to remove the residual metal ions. The solution was then heat-treated in a dry oven at 90 °C for 12 h to obtain the graphite oxide power, then 250 mg graphite oxide power were added to 200 ml DI water, were vigorously stirred for 30 min, and were then ultrasonicated (using Ultrasonic Processor, VCX 750) for 2 h. Finally, the resulting solution was refined and washed several times with hot water and kept in a dry oven for 6 h to obtain the graphene oxide powder.

Preparation of the WSe_2 composite. In a typical synthesis process, 0.675 g tungsten (vi) oxide (WO_3) are dispersed in deionized water, 0.5 M nitric acid are then added drop wise in a three-necked flask (100 mL), and the mixture is heated to 120 °C to eliminate H_2O and O_2. In a separate flask, 1.5 g of anhydrous sodium sulfite (Na_2SO_3) and 0.3 g crude selenium (Se) powder were dispersed in 200 ml of ethylene glycol with continuous magnetic stirring at 80 °C until a selenium salt was obtained. In the next step, both solutions are transferred to a stainless steel autoclave with a Teflon liner with 20 mL capacity for 24 h at 250 °C in an electric furnace. Finally, the WSe_2 precipitates are cooled to room temperature, the prepared solution is filtered using 47-mm Whatman filter paper, and the remaining material is heated to a temperature of 350 K for 12 h to obtain a WSe_2 power.

Preparation of WSe_2-graphene nanocomposite. Graphene oxide (200 mg) was added in 150 ml ethylene glycol and was then exfoliated to generate a graphene oxide nanosheet (GONS) dispersion solution via ultrasonication for 30 min. The WSe_2 powder from the above solution is mixed at equal volumetric ratios of 1:1, and the mixture is sonicated at room temperature for 6 h using a controllable serial-ultrasonic apparatus (Ultrasonic Processor, VCX 750, 500 Watt, Korea, Power 500 Watt, frequency 20 KHz, Amplitude 50%, low intensity). The reaction solution was allowed to cool and settle at room temperature after filtering with 47-mm Whatman filter paper with a pore size of 0.7 mm. The resulting powder was washed with distilled water multiple times and was dried in a vacuum oven at 80 °C for 12 h before heat treatment at 500 °C for 1 h with (Ar) inert atmosphere. The prepared sample was then labeled as WSe_2-graphene.

Characterization. The crystal structure and morphology of the prepared samples were measured using monochromatic high intensity Cu Kα radiation (λ = 1.5406 Å) in XRD (Shimadzu XD-D1), Energy dispersive X-ray spectrometer (EDX) was used to measure the atomic percentage of W, Se, and C elements, SEM (JSM-5600 JEOL, Japan) and TEM (JEOL, JEM-2010, and Japan) observations. X-ray photoelectron spectroscopy (XPS) was performed using a VG Scientific VISACA Lab 2000 device with a monochromatic Mg X-ray radiation source, and the Raman spectra of the prepared samples were observed using a spectrometer (Jasco Model Name NRS-3100) with an excitation laser wavelength of 532.06 nm. For quantitative analysis of the CH_3OH, a Standard Gas Chromatograph-Mass Spectrometer (GCMS-QP2010 SE) was used with a long column. Photoelectrochemical measurements were performed using a self-made photoelectrochemical system installed a 250-W halogen lamp as the irradiation source. The photocurrent measurement was performed by a computer-controlled Versa-STAT-3 electrochemical analyzer. A WSe_2-graphene modified photoelectrode with an active area of 1 cm^2 was used as the working electrode, and a Pt wire and saturated Ag/AgCl were used as the counter and reference electrodes, respectively. All the photocurrent measurements were conducted by dipping the WSe_2-graphene modified photoelectrode into a mixture of 0.1 M KCl and 0.5 M TEA at a constant potential of 0 V vs. Ag/AgCl.

Photocatalytic reduction of CO_2. The reduction of CO_2 with H_2O in the photocatalytic experiments was carried in a reactor designed in our laboratory, as shown in Fig. 1. The reactor consists of three parts: (1) light source, (2) closed chamber, (30 cm length × 2.0 diameter), (3) $CO_2 + N_2$ gas (N_2 gas was used to remove gasses from the reactor). 100 mg of photocatalyst (WSe_2-graphene) and Na_2SO_3 as hole scavenger[59] were added in 20 ml distilled water containing sodium bicarbonate ($NaHCO_3$, 0.04 M) and were constantly stirred for one hour. Ultra-high-purity grade CO_2 gas was purged through the reactor for 30 min, and then the suspension solution was magnetically stirred and irradiated with visible light using a metal halide lamp (500 W, SOLAREDGE700, Perfect Light, China). The distance between the light source and the photocatalyst remained at 10 cm, and a heat sink was equipped in the left side of the chamber to remove the lamp heat. Furthermore, the temperatures inside the reactor were kept at 283.15 K. The reaction continued up to 48 h, and in every 12 h interval, the reactor was allowed to cool down naturally for CH_3OH desorption from the catalyst. Then, the reaction product was taken from the reactor for GC analysis (GCMS-QP2010 SE).

The reaction quantum yield (QE) is estimated using the CH_3OH yield, noting that six electrons are required to reduce CO_2 to CH_3OH. The equation is as follow.

$$\phi_{\text{Methanol}}(\%) = 100 \times (6 \times \text{mole of } CH_3OH \text{ yield}) / (\text{mole of proton absorbed by catalyte})$$

$$-\text{Mole of proton} = (I \times S)/(N_A \times E)$$

where: I is light intensity (0.12 mW cm^{-2})
S is the irradiated area of the reactor (30 cm × 15 cm)
E is the photon energy (4.97×10^{-19} J at 400 nm)
NA is Avogadro's constant ($6.02 \times 1023\ mol^{-1}$)

Conclusion

In summary, the TMDC (WSe_2) materials are attached to the graphene nanosheet via ultra-sonication. The SEM and TEM images of the prepared samples show that the WSe_2 have nanowire morphology that is uniformly distributed on the graphene sheets, and the average size of the nanowires is verified to be from 30 to 130 nm. The graphene sheet-supported WSe_2 nanowire resulting from the binary structure present excited charge carriers with the combined effect of WSe_2 and graphene, improving the recombination time. Raman spectroscopy and XPS measurements show an intimate contact and chemical binding interaction between the WS_2 and GO. Graphene plays a role as an electron mediator to support a binary system and to help provide stable photocatalyst materials. The CO_2 photo reduction experiment was carried out to investigate the photo catalytic reduction of CO_2 with the WSe_2-G nanocomposite, achieving a maximum photocatalytic efficiency after 48 h. The WSe_2-graphene with added Na_2SO_3 (48 h) showed the highest photocatalytic efficacy and obtained a total CH_3OH yield of 5.0278 µmol $g^{-1}h^{-1}$. Our present work indicates that the attachment of WSe_2 on the graphene sheet can further increase the photocatalytic performance, opening new ways to deploy novel, next-generation heterojunction photocatalysts for environmentally-related applications.

References

1. Lacis, A. A., Schmidt, G. A., Rind, D. & Ruedy, R. A. Atmospheric CO_2: Principal control knob governing Earth's temperature. *Science* **330**, 356–359, doi:10.1126/science.1190653 (2010).
2. Yu, J., Low, J., Xiao, W., Zhou, P. & Jaroniec, M. Enhanced photocatalytic CO_2-reduction activity of anatase TiO_2 by coexposed {001} and {101} facets. *Journal of the American Chemical Society* **136**, 8839–8842, doi:10.1021/ja5044787 (2014).
3. Maginn, E. J. What to Do with CO_2. *The Journal of Physical Chemistry Letters* **1**, 3478–3479, doi:10.1021/jz101582c (2010).
4. Li, X., Wen, J., Low, J., Fang, Y. & Yu, J. Design and fabrication of semiconductor photocatalyst for photocatalytic reduction of CO_2 to solar fuel. *Science China Materials* **57**, 70–100, doi:10.1007/s40843-014-0003-1 (2014).
5. Habisreutinger, S. N., Schmidt-Mende, L. & Stolarczyk, J. K. Photocatalytic reduction of CO_2 on TiO_2 and other semiconductors. *Angewandte Chemie International Edition* **52**, 7372–7408, doi:10.1002/anie.201207199 (2013).
6. Ramesha, G. K., Brennecke, J. F. & Kamat, P. V. Origin of catalytic effect in the reduction of CO_2 at nanostructured TiO_2 films. *ACS Catalysis* **4**, 3249–3254, doi:10.1021/la5009076 (2014).
7. Yuan, L. & Xu, Y.-J. Photocatalytic conversion of CO_2 into value-added and renewable fuels. *Applied Surface Science* **342**, 154–167, doi:10.1016/j.apsusc.2015.03.050 (2015).
8. Yu, J., Wang, K., Xiao, W. & Cheng, B. Photocatalytic reduction of CO_2 into hydrocarbon solar fuels over g-C3N4–Pt nanocomposite photocatalysts. *Physical Chemistry Chemical Physics* **16**, 11492–11501, doi:10.1039/c4cp00133h (2014).
9. Ehsan, M. F. & He, T. *In situ* synthesis of ZnO/ZnTe common cation heterostructure and its visible-light photocatalytic reduction of CO_2 into CH_4. *Applied Catalysis B: Environmental* **166**, 345–352, doi:10.1016/j.apcatb.2014.11.058 (2015).
10. Marszewski, M., Cao, S., Yu, J. & Jaroniec, M. Semiconductor-based photocatalytic CO_2 conversion. *Materials Horizons* **2**, 261–278, doi:10.1039/C4MH00176A (2015).
11. Cojocaru, B. *et al*. Band gap effect on the photocatalytic activity of supramolecular structures obtained by entrapping photosensitizers in different inorganic supports. *Physical Chemistry Chemical Physics* **11**, 5569–5577, doi:10.1039/b902348h (2009).
12. Voiry, D. *et al*. Enhanced catalytic activity in strained chemically exfoliated WS_2 nanosheets for hydrogen evolution. *Nature materials* **12**, 850–855, doi:10.1038/nmat3700 (2013).
13. Kibsgaard, J., Chen, Z., Reinecke, B. N. & Jaramillo, T. F. Engineering the surface structure of MoS_2 to preferentially expose active edge sites for electrocatalysis. *Nature materials* **11**, 963–969, doi:10.1038/nmat3439 (2012).
14. Cheng, L. *et al*. Ultrathin WS_2 nanoflakes as a high-performance electrocatalyst for the hydrogen evolution reaction. *Angewandte Chemie International Edition* **53**, 7860–7863, doi:10.1002/anie.201402315 (2014).
15. Lukowski, M. A. *et al*. Enhanced hydrogen evolution catalysis from chemically exfoliated metallic MoS_2 nanosheets. *Journal of the American Chemical Society* **135**, 10274–10277, doi:10.1021/ja404523s (2013).
16. Li, H. *et al*. Mechanical Exfoliation and Characterization of Single-and Few-Layer Nanosheets of WSe_2, TaS_2, and $TaSe_2$. *Small* **9**, 1974–1981, doi:10.1002/smll.v9.11 (2013).
17. Matte, H. R., Plowman, B., Datta, R. & Rao, C. Graphene analogues of layered metal selenides. *Dalton Transactions* **40**, 10322–10325, doi:10.1039/c1dt10652j (2011).
18. Wang, Q. H., Kalantar-Zadeh, K., Kis, A., Coleman, J. N. & Strano, M. S. Electronics and optoelectronics of two-dimensional transition metal dichalcogenides. *Nature nanotechnology* **7**, 699–712, doi:10.1038/nnano.2012.193 (2012).
19. Cao, L. *et al*. Direct Laser-Patterned Micro-Supercapacitors from Paintable MoS2 Films. *Small* **9**, 2905–2910, doi:10.1002/smll.v9.17 (2013).
20. Chen, D. *et al*. *In situ* nitrogenated graphene–few-layer WS_2 composites for fast and reversible Li^+ storage. *Nanoscale* **5**, 7890–7896, doi:10.1039/c3nr02920d (2013).
21. Yin, Z. *et al*. Single-layer MoS_2 phototransistors. *ACS nano* **6**, 74–80, doi:10.1021/nn2024557 (2011).
22. Li, Y., Li, Y.-L., Araujo, C. M., Luo, W. & Ahuja, R. Single-layer MoS_2 as an efficient photocatalyst. *Catalysis Science & Technology* **3**, 2214–2220 (2013).
23. Li, Y. *et al*. MoS_2 nanoparticles grown on graphene: an advanced catalyst for the hydrogen evolution reaction. *Journal of the American Chemical Society* **133**, 7296–7299, doi:10.1021/ja201269b (2011).
24. Merki, D., Fierro, S., Vrubel, H. & Hu, X. Amorphous molybdenum sulfide films as catalysts for electrochemical hydrogen production in water. *Chemical Science* **2**, 1262–1267, doi:10.1039/C1SC00117E (2011).
25. Chang, H. & Wu, H. Graphene-based nanocomposites: preparation, functionalization, and energy and environmental applications. *Energy & Environmental Science* **6**, 3483–3507 (2013).
26. Zhang, H. *et al*. Large-Scale Production of Nanographene Sheets with a Controlled Mesoporous Architecture as High-Performance Electrochemical Electrode Materials. *Chem Sus Chem* **6**, 1084–1090, doi:10.1002/cssc.v6.6 (2013).
27. Liang, Y. T., Vijayan, B. K., Gray, K. A. & Hersam, M. C. Minimizing graphene defects enhances titania nanocomposite-based photocatalytic reduction of CO_2 for improved solar fuel production. *Nano letters* **11**, 2865–2870, doi:10.1021/nl2012906 (2011).
28. Liu, Z. *et al*. Assembled 3D electrocatalysts for efficient hydrogen evolution: WSe_2 layers anchored on graphene sheets. *Inorganic Chemistry Frontiers* **3**, 313–319, doi:10.1039/C5QI00216H (2016).
29. Guo, J., Shi, Y., Bai, X., Wang, X. & Ma, T. Atomically thin $MoSe_2$/graphene and WSe_2/graphene nanosheets for the highly efficient oxygen reduction reaction. *Journal of Materials Chemistry A* **3**, 24397–24404, doi:10.1039/C5TA06909B (2015).
30. Chakravarty, D. & Late, D. J. Microwave and hydrothermal syntheses of WSe_2 micro/nanorods and their application in supercapacitors. *RSC Advances* **5**, 21700–21709, doi:10.1039/C4RA12599A (2015).
31. Bourlinos, A. B. *et al*. Graphite oxide: chemical reduction to graphite and surface modification with primary aliphatic amines and amino acids. *Langmuir* **19**, 6050–6055, doi:10.1021/la026525h (2003).

32. Kovtyukhova, N. I. *et al.* Layer-by-layer assembly of ultrathin composite films from micron-sized graphite oxide sheets and polycations. *Chemistry of Materials* **11**, 771–778, doi:10.1021/cm981085u (1999).
33. Ai, W. *et al.* Nitrogen and sulfur codoped graphene: multifunctional electrode materials for high-performance Li-ion batteries and oxygen reduction reaction. *Advanced Materials* **26**, 6186–6192, doi:10.1002/adma.201401427 (2014).
34. Shi, Y. *et al.* van der Waals epitaxy of MoS_2 layers using graphene as growth templates. *Nano letters* **12**, 2784–2791, doi:10.1021/nl204562j (2012).
35. Wang, H., Robinson, J. T., Diankov, G. & Dai, H. Nanocrystal growth on graphene with various degrees of oxidation. *Journal of the American Chemical Society* **132**, 3270–3271, doi:10.1021/ja100329d (2010).
36. Wang, H. *et al.* Mn_3O_4− graphene hybrid as a high-capacity anode material for lithium ion batteries. *Journal of the American Chemical Society* **132**, 13978–13980, doi:10.1021/ja105296a (2010).
37. Muscuso, L., Cravanzola, S., Cesano, F., Scarano, D. & Zecchina, A. Optical, Vibrational, and structural properties of MoS_2 nanoparticles obtained by exfoliation and fragmentation via ultrasound cavitation in isopropyl alcohol. *The Journal of Physical Chemistry C* **119**, 3791–3801, doi:10.1021/jp511973k (2015).
38. Yu, J. H. *et al.* Vertical heterostructure of two-dimensional MoS_2 and WSe_2 with vertically aligned layers. *Nano letters* **15**, 1031–1035, doi:10.1021/nl503897h (2015).
39. Wang, R.-C., Chen, Y.-C., Chen, S.-J. & Chang, Y.-M. Unusual functionalization of reduced graphene oxide for excellent chemical surface-enhanced Raman scattering by coupling with ZnO. *Carbon* **70**, 215–223, doi:10.1016/j.carbon.2013.12.110 (2014).
40. Dresselhaus, M. S., Jorio, A., Hofmann, M., Dresselhaus, G. & Saito, R. Perspectives on carbon nanotubes and graphene Raman spectroscopy. *Nano letters* **10**, 751–758, doi:10.1021/nl904286r (2010).
41. Huang, T. *et al.* The effects of low power density CO_2 laser irradiation on graphene properties. *Applied Surface Science* **273**, 502–506, doi:10.1016/j.apsusc.2013.02.069 (2013).
42. Wang, Y. Y. *et al.* Raman studies of monolayer graphene: the substrate effect. *The Journal of Physical Chemistry C* **112**, 10637–10640, doi:10.1021/jp8008404 (2008).
43. Ullah, K., Lei, Z., Ye, S., Ali, A. & Oh, W.-C. Microwave synthesis of a $CoSe_2$/graphene–TiO_2 heterostructure for improved hydrogen evolution from aqueous solutions in the presence of sacrificial agents. *RSC Advances* **5**, 18841–18849, doi:10.1039/C5RA00065C (2015).
44. Katrib, A., Hemming, F., Wehrer, P., Hilaire, L. & Maire, G. The multi-surface structure and catalytic properties of partially reduced WO_3, WO_2 and WC + O_2 or W + O_2 as characterized by XPS. *Journal of electron spectroscopy and related phenomena* **76**, 195–200, doi:10.1016/0368-2048(95)02451-4 (1995).
45. Wang, H. *et al.* $MoSe_2$ and WSe_2 nanofilms with vertically aligned molecular layers on curved and rough surfaces. *Nano letters* **13**, 3426–3433, doi:10.1021/nl401944f (2013).
46. Abdallah, We. A. & Nelson, A. Characterization of $MoSe_2$ (0001) and ion-sputtered $MoSe_2$ by XPS. *Journal of materials science* **40**, 2679–2681, doi:10.1055/s-0029-1185676 (2005).
47. Boscher, N. D., Carmalt, C. J. & Parkin, I. P. Atmospheric pressure chemical vapor deposition of WSe_2 thin films on glass—highly hydrophobic sticky surfaces. *Journal of Materials Chemistry* **16**, 122–127, doi:10.1039/B514440J (2006).
48. Szabó, T. *et al.* Evolution of surface functional groups in a series of progressively oxidized graphite oxides. *Chemistry of materials* **18**, 2740–2749, doi:10.1021/cm060258+ (2006).
49. Jeong, H.-K. *et al.* X-ray absorption spectroscopy of graphite oxide. *EPL (Europhysics Letters)* **82**, 67004, doi:10.1209/0295-5075/82/67004 (2008).
50. Dreyer, D. R., Park, S., Bielawski, C. W. & Ruoff, R. S. The chemistry of graphene oxide. *Chemical Society Reviews* **39**, 228–240, doi:10.1039/b917103g (2010).
51. Zhang, L.-f & Zhang, C.-y Multifunctional Co 0.85 Se/graphene hybrid nanosheets: controlled synthesis and enhanced performances for the oxygen reduction reaction and decomposition of hydrazine hydrate. *Nanoscale* **6**, 1782–1789, doi:10.1039/c3nr05509d (2014).
52. Wan, D. *et al.* Low-temperature aluminum reduction of graphene oxide, electrical properties, surface wettability, and energy storage applications. *ACS nano* **6**, 9068–9078, doi:10.1021/nn303228r (2012).
53. Zang, Y., Lei, J., Hao, Q. & Ju, H. "Signal-On" Photoelectrochemical Sensing Strategy Based on Target-Dependent Aptamer Conformational Conversion for Selective Detection of Lead (II) Ion. *ACS applied materials & interfaces* **6**(18), 15991–15997, doi:10.1021/am503804g (2014).
54. Bonaccorso, F., Sun, Z., Hasan, T. & Ferrari, A. Graphene photonics and optoelectronics. *Nature photonics.* **4**(9), 611–622, doi:10.1038/nphoton.2010.186 (2010).
55. Zeng, P., Zhang, Q., Peng, T. & Zhang, X. One-pot synthesis of reduced graphene oxide-Cadmium sulfide nanocomposite and its photocatalytic hydrogen production. *Physical Chemistry Chemical Physics* **13**, 21496–21502 (2011).
56. Ali, A. & Oh, W.-C. Catalytic reduction of CO_2 to alcohol with Cu_2Se-combined graphene binary nanocomposites. *Fullerenes, Nanotubes and Carbon Nanostructures* **24**, 555–563, doi:10.1080/1536383X.2016.1205036 (2016).
57. Oh, W.-c & Zhang, F.-j Preparation and characterization of graphene oxide reduced from a mild chemical method. *Asian Journal of Chemistry* **23**, 875 (2011).
58. Chen, M.-L., Park, C.-Y., Choi, J.-G. & Oh, W.-C. Synthesis and characterization of metal (Pt, Pd and Fe)-graphene composites. *Journal of the Korean Ceramic Society* **48**, 147–151, doi:10.4191/KCERS.2011.48.2.147 (2011).
59. Zhai, Q. *et al.* Photocatalytic conversion of carbon dioxide with water into methane: platinum and copper (I) oxide co-catalysts with a core–shell structure. *Angewandte Chemie* **125**, 5888–5891, doi:10.1002/ange.201301473 (2013).

Author Contributions

W.C. Oh proposed and supervised the project; Asghar Ali designed and performed the experiments. Asghar Ali analyzed the data and wrote the manuscript. All authors participated in the discussions and provided input on the manuscript.

Additional Information

Competing Interests: The authors declare that they have no competing interests.

Publisher's note: Springer Nature remains neutral with regard to jurisdictional claims in published maps and institutional affiliations.